Climate velocity in inland standing waters

Article

Accepted Version

Title: Climate velocity in inland standing waters

Authors: R. Iestyn Woolway[1,2*], Stephen C. Maberly[3]

Affiliations:
[1]Centre for Freshwater and Environmental Studies, Dundalk Institute of Technology, Dundalk, Ireland
[2]European Space Agency Climate Office, ECSAT, Harwell Campus, Didcot, Oxfordshire, UK
[3]UK Centre for Ecology & Hydrology, Lancaster Environment Centre, Lancaster, UK

*Correspondence to: riwoolway@gmail.com

First paragraph: Inland standing waters are particularly vulnerable to increasing water temperature. Here, using a high-resolution numerical model, we find that the velocity of climate change in the surface of inland standing waters globally was 3.5±2.3 km decade^{-1} from 1861-2005, which is similar to, or lower than, rates of active dispersal of some motile species. However, from 2006-2099, the velocity of climate change will increase to 8.7±5.5 km decade^{-1} under a low emission pathway (RCP 2.6) and 57.0±17.0 km decade^{-1} under a high emission pathway (RCP 8.5), meaning that thermal habitat in inland standing waters will move faster than the ability of some species to disperse to cooler areas. The fragmented distribution of standing waters in a landscape will restrict redistribution, even for species with a high dispersal ability, so that the negative consequences of rapid warming for freshwater species are likely to be much greater than for terrestrial and marine realms.

Main Text: Inland standing waters hold a large majority of the Earth's liquid surface fresh water, support important biodiversity, and provide key ecosystem services to people around the world[1]. Yet, standing waters are highly vulnerable to climate change. Some of the most pervasive and concerning consequences of climatic change on standing waters are the direct and indirect effects of rising water temperature[2]. This temperature increase can influence physical structure, rates of processes and species composition[5,6] and, in turn, temperature can strongly influence the distribution and abundance of freshwater species across the globe[7]. However, within a lake or reservoir, temperature varies seasonally[8], horizontally[9] and often vertically in those that are deep enough to stratify[10,11]. As standing waters warm over time, aquatic communities may have to disperse to track thermally suitable habitats[4]. A critical step in the understanding of climate change impacts on aquatic ecosystems is therefore to describe the speed at which their thermal environment is changing, often referred to as the velocity of climate change, i.e., the distance at which isotherms shift over time[3]. The velocity of climate change has been studied extensively in marine and terrestrial ecosystems[12,13], but has not yet been investigated in standing waters globally, despite the vulnerability of freshwater species to direct and indirect thermal alterations associated with warming[14].

The velocity of climate change (km decade^{-1}) is calculated as the quotient of the long-term temperature trend (°C decade^{-1}) to the two-dimensional spatial gradient in temperature (°C km^{-}

[1]). In this study, we calculated the distribution of the historic velocity of climate change in the surface of inland standing waters worldwide using surface temperatures from a new state-of-the-art global reanalysis from the European Centre for Medium-Range Weather Forecasts (ECMWF), ERA5, on a 0.25°-by-0.25° grid (see Supplementary Material). Inland water temperature within ERA5 is simulated via the Freshwater Lake model, FLake, which is embedded as a tile in the Tiled ECMWF Scheme for Surface Exchanges over Land incorporating land surface hydrology (HTESSEL). The FLake model has been extensively validated here (Extended Data Fig. 1) and in simulations of the surface temperature of inland waters globally and has been used to quantify worldwide aspects of inland water thermal dynamics such as seasonal cycles[8], onset of summer stratification[5], and mixing dynamics[9].

Our study demonstrates that over a period of 40 years (1979-2018), the annual surface temperature of inland standing waters has increased in 99% of the surface grid-cells analyzed, although there were substantial regional variations in magnitude (Fig. 1a). Worldwide, the median rate of warming in inland standing waters was 0.13 °C decade^{-1} (Fig. 1a). Our computed trends are similar to those calculated in previous studies which have demonstrated that the vast majority of lakes worldwide are warming[2], despite differences in the seasonal extent of the data (all year *vs* summer) or the range of years analysed. Across inland standing waters, the median spatial gradient in temperature was 0.009 °C km^{-1} (Fig. 1b) and it was greater in regions with large elevation gradients, such as in the European Alps (Extended Data Figs 2-3). When the rate of warming is combined with the spatial gradient in temperature, the resulting median velocity of climate change across standing waters worldwide was 13.94 km decade^{-1} during 1979-2018 (Fig. 1c). As a result of higher increases in surface temperatures and a lower spatial gradient, the velocity of climate change is greater at mid- to high-latitude (Fig. 1d) and in regions with low gradients in elevation (Extended Data Figs 2, 4).

We compared the velocity of climate change in inland standing waters from 1979 to 2018 to those calculated for marine and terrestrial ecosystems[3, 12] by applying the same climate velocity algorithm to surface air temperatures over land and sea surface temperatures, both of which are available from ERA5. We find that the velocity of climate change in inland standing waters was comparable to that calculated for surface air temperatures over land (13.76 km decade^{-1}), despite the median rate of warming in the latter being twice as fast (0.26 *vs* 0.13 °C decade^{-1}) (Fig. 2). The velocity of climate change in the ocean (26.84 km decade^{-1}), as calculated from sea surface temperatures, was higher than in standing waters and over land, because of the smaller spatial temperature gradient (0.003 °C km^{-1}). The spatial temperature gradient in the ocean was a third of the spatial temperature gradient in standing waters (0.009 °C km^{-1}) and nearly a sixth of that over land (0.017 °C km^{-1}). The velocity of climate change in the ocean is much less variable than in inland waters or on land (Fig. 2e) with small gradients punctuated by sharp thermal boundaries (e.g., see the Gulf Stream). Areas of high velocity extend across larger regions in the ocean compared to the other ecosystems.

The climate velocities for inland standing waters calculated from ERA5 cannot be extended into the future, as the ERA5 temperatures are produced in near real-time as an operational forecast. To project future changes in climate velocities, a different approach is required. In

this study, we simulate the velocity of climate change during the 21st century using the same water temperature model as used in ERA5 during 1979-2018 (i.e., FLake), but now force the model with bias-corrected climate projections from four global climate models: MIROC5, IPSL-CM5A-LR, GFDL-ESM2M and HadGEM2-ES (see Supplementary Material), on a 0.5°-by-0.5° grid. These climate models contributed to phase 5 of the Coupled Model Intercomparison Project (CMIP5) and were bias-corrected within the Inter-Sectoral Impact Model Intercomparison Project (ISIMIP2b). Contemporary to future projections (2006 – 2099) for low, medium and high Representative Concentration Pathway (RCP) scenarios are investigated: RCP 2.6, 6.0 and 8.5 respectively (Fig. 3). For comparison, and to extend the record back in time, we also calculate the velocity of climate change from 1861-2005, where the historic climate simulations were forced using anthropogenic greenhouse gas and aerosol forcing in addition to natural forcing.

The magnitude of surface air temperature change, which is one of the dominant drivers of surface warming in standing waters, increases considerably during the 21st century, with the magnitude of change increasing from RCP 2.6 to 6.0 to 8.5 (Extended Data Fig. 5). Our simulations demonstrate that the surface temperature of global standing waters will also increase during the 21st century (Fig. 3a). Specifically, under RCP 2.6, 6.0, and 8.5, surface water temperature trends will accelerate to 0.06±0.04 °C decade^{-1} (quoted uncertainties represent the standard deviation from the lake model driven by all four climate model projections), 0.23±0.07 °C decade^{-1}, and 0.40±0.12 °C decade^{-1}, respectively (Fig. 3b) from 2006 to 2099, compared to 0.03±0.02 °C decade^{-1} from 1861-2005. Note that the temperature trend calculated from 1861-2005 is lower than that reported previously for the 1979-2018 period due to the rapid warming which occurred following the 1980s (Fig. 3a), in agreement with previous studies of observed lake surface temperature change[15]. The spatial gradient in temperature is similar across the different future climate scenarios (Fig. 3c), as well as the 1861-2005 period. Specifically, the spatial gradient was 0.0063±0.00004 °C km^{-1} during the historic period, and marginally higher during the 21st century at 0.0064±0.00005 °C km^{-1} under RCP 2.6 and 6.0, and 0.0065±0.00009 °C km^{-1} under RCP 8.5. The model projections demonstrate that the median velocity of climate change from 1861-2005 was 3.5±2.3 km decade^{-1}, again lower than the 1979-2018 period due to the different temporal period considered. We project a median climate velocity during the period 2006-2099 of 8.7±5.5 km decade^{-1} for RCP 2.6, 32.6±10.3 km decade^{-1} for RCP 6.0 and 57.0±17.0 km decade^{-1} for RCP 8.5.

The worldwide patterns of climate velocities are projected largely to hold under 21st century climate change, with areas that have experienced the highest velocities during the historic period (1861-2005) also typically experiencing the greatest velocities during the contemporary to future period (2006-2099). Specifically, there were statistically significant relationships between the worldwide climate velocities during the historic and future periods under RCP 2.6 ($R^2 = 0.52$; $p < 0.001$), RCP 6.0 ($R^2 = 0.48$; $p < 0.001$), and RCP 8.5 ($R^2 = 0.38$; $p < 0.001$), but with a decrease in correlation with an increase in the severity of climate change. There appear to be no systematic changes in the projected spatial patterns of climate velocity in the future; but some regions, such as northern Europe, northeastern USA and northern Canada,

will experience greater changes than others (Extended Data Fig. 6). The velocity of climate change in standing waters during the 21st century will be slightly greater in summer than in winter (Fig. 3e-g; summer was defined as July-September in the Northern Hemisphere and January-March in the Southern Hemisphere, and the opposite definition was used for winter). For example, under RCP 8.5, our simulations suggest that by the end of the current century the median velocity of climate change will increase to 58.0±13.2 km decade^{-1} during summer and 43.2±10.5 km decade^{-1} during winter. This is a result of surface water temperatures in standing waters increasing at a faster rate in summer (0.59±0.14 °C decade^{-1}) than in winter (0.47±0.11 °C decade^{-1}), but is also influenced by a slightly higher median spatial temperature gradient between summer (0.008±0.00007 °C km^{-1}) and winter (0.007±0.00007 °C km^{-1}) (Fig. 3).

The pace of climate change identified here for standing waters during the 21st century will produce new, and rapidly warming, thermal conditions for species at a given location. The ecological consequences will depend on the ability of a species to survive at a site, disperse within a catchment or disperse between catchments. The ability of a species to continue to survive at a site will depend on the temperature sensitivity of their most susceptible life-stages[16,17]. In addition, phenotypic plasticity may allow a species to acclimate to higher temperatures while adaptation to higher temperatures is unlikely since rates of evolutionary change for critical thermal maxima are many orders of magnitude lower than even the rate of historical temperature trends[2,18]. In addition, cooler water at depth during seasonal stratification may provide a potential refuge from increasing surface water temperatures. However, the environment at depth may not always be suitable in terms of light, food supply or oxygen concentration. For example, some fish are unable to exploit cooler temperatures at depth because of low oxygen concentration[19], and oxygen-depletion is likely to increase with climate change and continued eutrophication. Furthermore, the critical thermal period may occur in non-stratified periods of the year. For example, early life stages can be the most temperature sensitive[16] and these can occur in the winter when stratification is generally absent, but the velocity of climate change is almost as great as in the summer. The evidence of summer fish-kills in lakes, and their lack of correlation with lake depth, suggests that depth may only provide a partial thermal refuge[6] and, as demonstrated in the oceans, climate velocities can be faster at depth than at the surface[20]. Phenological change in response to warming may allow sensitive stages to exploit cooler times of year, but where seasonality of different components of the food-web changes at different rates the changing phenology could also cause food-web desynchronization, with potential negative consequences[21]. While there has been a focus on the consequence of rapid surface warming of inland standing waters for cold-water stenotherms at high latitudes[22], warm-water species that are close to their critical thermal limit at low latitudes are equally at risk[23].

Dispersal is an important life-history trait that, unlike the responses above, will not prevent species loss at a given site but may permit a species to survive by moving to cooler habitats. Within the dendritic hydrological network of a catchment, dispersal to cooler standing water can occur either upstream to higher elevations or, in large river systems, downstream to higher latitudes. However, species in headwaters or isolated tributaries may have a low connectivity to more suitable habitats and so be particularly susceptible to rapid warming[24]. For some

species, such as freshwater molluscs, rates of active dispersal of 1 to 10 km decade^{-1} (ref. 25) are less than forecast future change under both medium and high greenhouse gas concentration pathways. While many amphibians move relatively small distances, at least some individuals may move over 10 km (ref. 26). More motile species, such as some fish, have the potential to migrate rapidly in response to long-term climate change[4,27]. However, in all cases, dispersal may be limited by physical and ecological barriers caused by the complex mosaic of freshwater environments. The increasing number of dams on the world's rivers[28] may restrict dispersal further by preventing access to upstream reaches and because the habitat in the intervening reservoir may be unsuitable. Even greater challenges are faced in dispersal across land to cooler catchments at higher elevation or higher latitude as illustrated by the fragmented distribution of fish within a landscape[29] and the high degree of endemism in freshwater organisms[30]. Aquatic insects have a variable potential to disperse actively between catchments in their adult stage[31], while other organisms depend on vectors such as wind or transport by large motile animals such as birds[32]. For dispersal within and between catchments, colonization and expansion in cooler areas may be impeded by interactions with the resident community of species that can restrict the establishment of new species despite an adequate propagule pressure[32].

The discussion above outlines the challenges that species in inland waters face in responding to rapid climate change. Although the velocity of climate change of inland standing waters is about half that of the ocean, the future consequences for the conservation of species, and the goods and services they provide, is likely to be much greater. This is caused by the combination of low dispersal rates of some freshwater species, substantial barriers to dispersal and ongoing major disruption to inland water biodiversity and ecosystem function by multiple anthropogenic stressors[30]. A recent analysis showed that the tracking of isothermal shifts in latitude in terrestrial species was six-times slower than in marine species[33]; this tracking is likely to be even slower for species from inland standing waters. Placing this global analysis in a conservation context, will require information on the thermal tolerance of different freshwater species, their dispersal ability and the local and regional connectivity of their habitat. It will also require the more complex interactions between species within a community to be understood and, for species such as amphibians and some insects and fish with life stages in different environments, the consequences of environmental change experienced in different realms.

List of Figures

Fig. 1 | The velocity of climate change in the surface of standing waters (1979-2018). (a) The annual surface water temperature trend (°C decade^{-1}). **(b)** The two-dimensional spatial gradient of annual surface water temperature change (°C km^{-1}). **(c)** The velocity of temperature change determined from the quotient of **a** and **b** (km decade^{-1}). Latitudinal mean (black) and median (grey) of (**d**) the temperature trend, (**e**) the spatial temperature gradient and (**f**) the velocity of climate change. White regions represent those where standing waters are absent within the global database.

Fig. 2 | The velocity of climate change in terrestrial and marine ecosystems (1979-2018). (a) The annual temperature trend (°C decade^{-1}) in terrestrial (left) and marine (right) ecosystems. **(b)** The two-dimensional spatial gradient of annual surface temperature change (°C km^{-1}). **(c)** The velocity of temperature change determined from the quotient of **a** and **b** (km decade^{-1}). Comparison of the surface temperature trend (**d**), spatial temperature gradient (**e**), and velocity of climate change (**f**) in standing waters with those calculated over land (terrestrial) and in the ocean (marine). Each box represents the interquartile range, the horizontal line is the median, and the whiskers are 1.5 times the interquartile range.

Fig. 3 | Historic and future projections in the velocity of climate change in inland standing waters. (a) Temporal change in annual surface water temperature anomalies (relative to 1951-1980) from 1861-2099 showing the historic period (1861-2005), with contemporary to future climate projections (2006-2099) under three greenhouse gas concentration pathways (RCPs 2.6, 6.0, and 8.5). The thick lines show the average from the lake model driven by four global climate models (MIROC5, IPSL-CM5A-LR, GFDL-ESM2M and HadGEM2-ES), and the shaded regions represent the standard deviation. Also shown are model projections of **(b)** the temporal gradient of temperature change (°C decade^{-1}), **(c)** the two-dimensional spatial gradient of surface temperature change (°C km^{-1}), and **(d)** the velocity of climate change (km decade^{-1}). Panels **e-g** show equivalent data for winter *vs* summer. Each box represents the interquartile range, the horizontal line is the median, and the whiskers are 1.5 times the interquartile range. Each box contains the simulations from the lake model forced by each of the climate model projections.

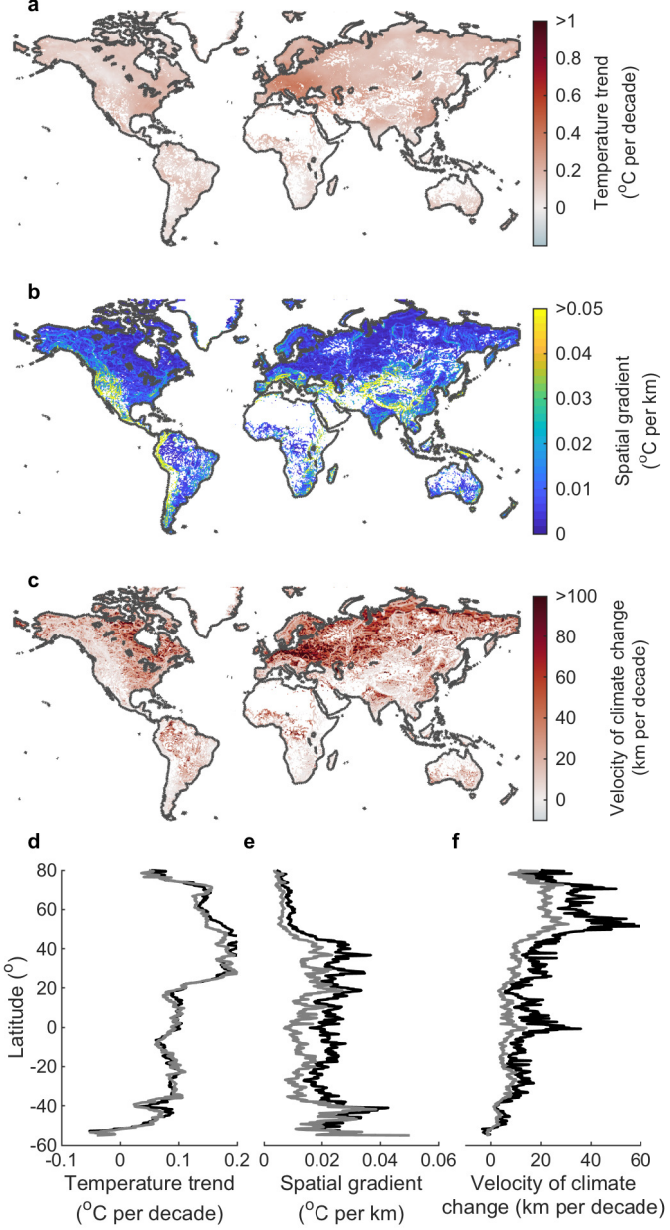
a
>1
0.8
0.6
0.4
0.2
0
Temperature trend
(°C per decade)
b
>0.05
0.04
0.03
0.02
0.01
0
Spatial gradient
(°C per km)
c
>100
80
60
40
20
0
Velocity of climate change
(km per decade)
d
e
f
Latitude (°)
80
60
40
20
0
-20
-40
-60
-0.1
0
0.1
0.2
Temperature trend
(°C per decade)
0
0.02
0.04
0.06
Spatial gradient
(°C per km)
0
20
40
60
Velocity of climate
change (km per decade)

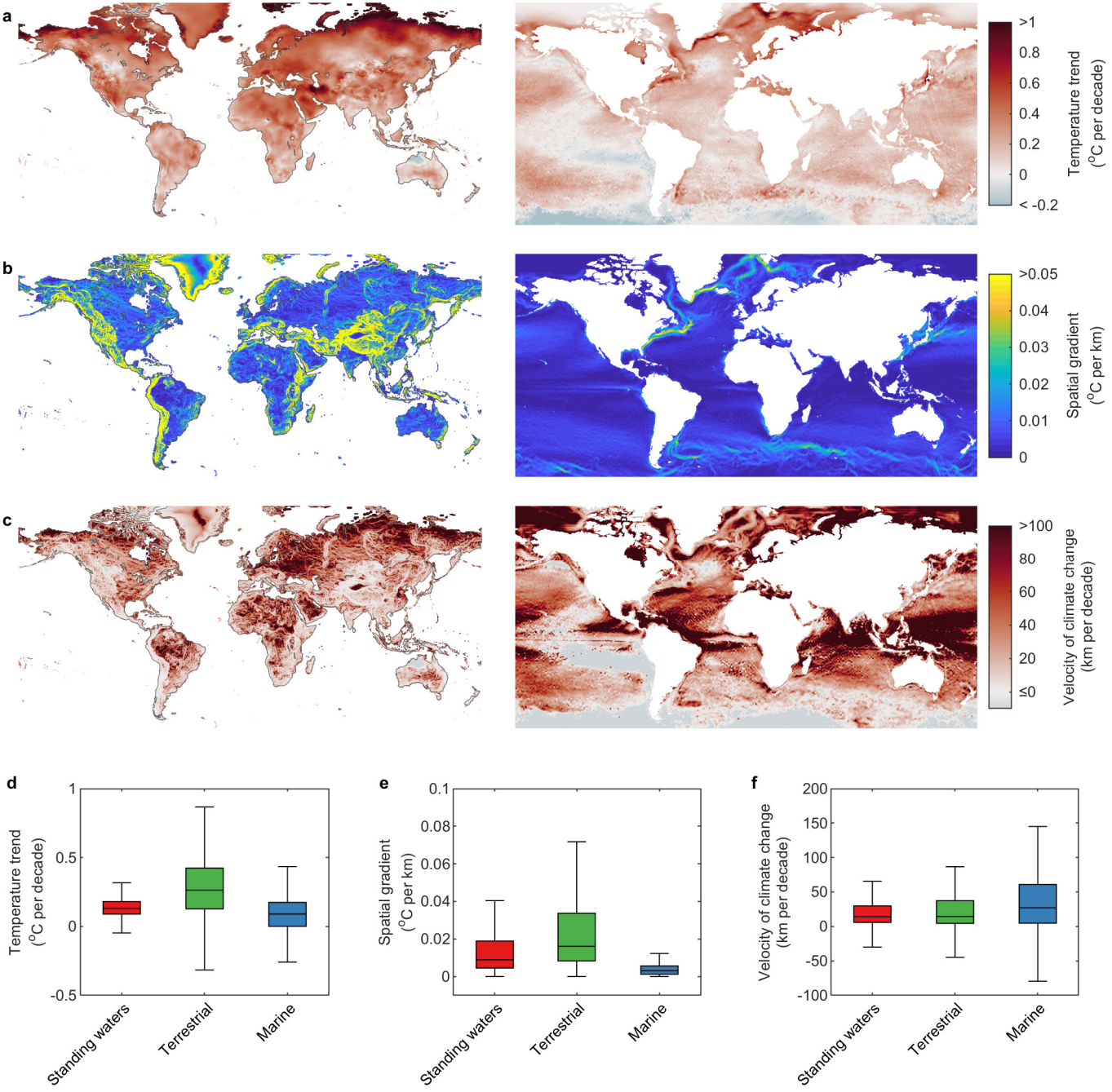
a
>1
0.8
0.6
0.4
0.2
0
< -0.2
Temperature trend
(°C per decade)
b
>0.05
0.04
0.03
0.02
0.01
0
Spatial gradient
(°C per km)
c
>100
80
60
40
20
≤0
Velocity of climate change
(km per decade)
d
Temperature trend
(°C per decade)
1
0.5
0
-0.5
Standing waters
Terrestrial
Marine
e
Spatial gradient
(°C per km)
0.1
0.08
0.06
0.04
0.02
0
Standing waters
Terrestrial
Marine
f
Velocity of climate change
(km per decade)
200
150
100
50
0
-50
-100
Standing waters
Terrestrial
Marine

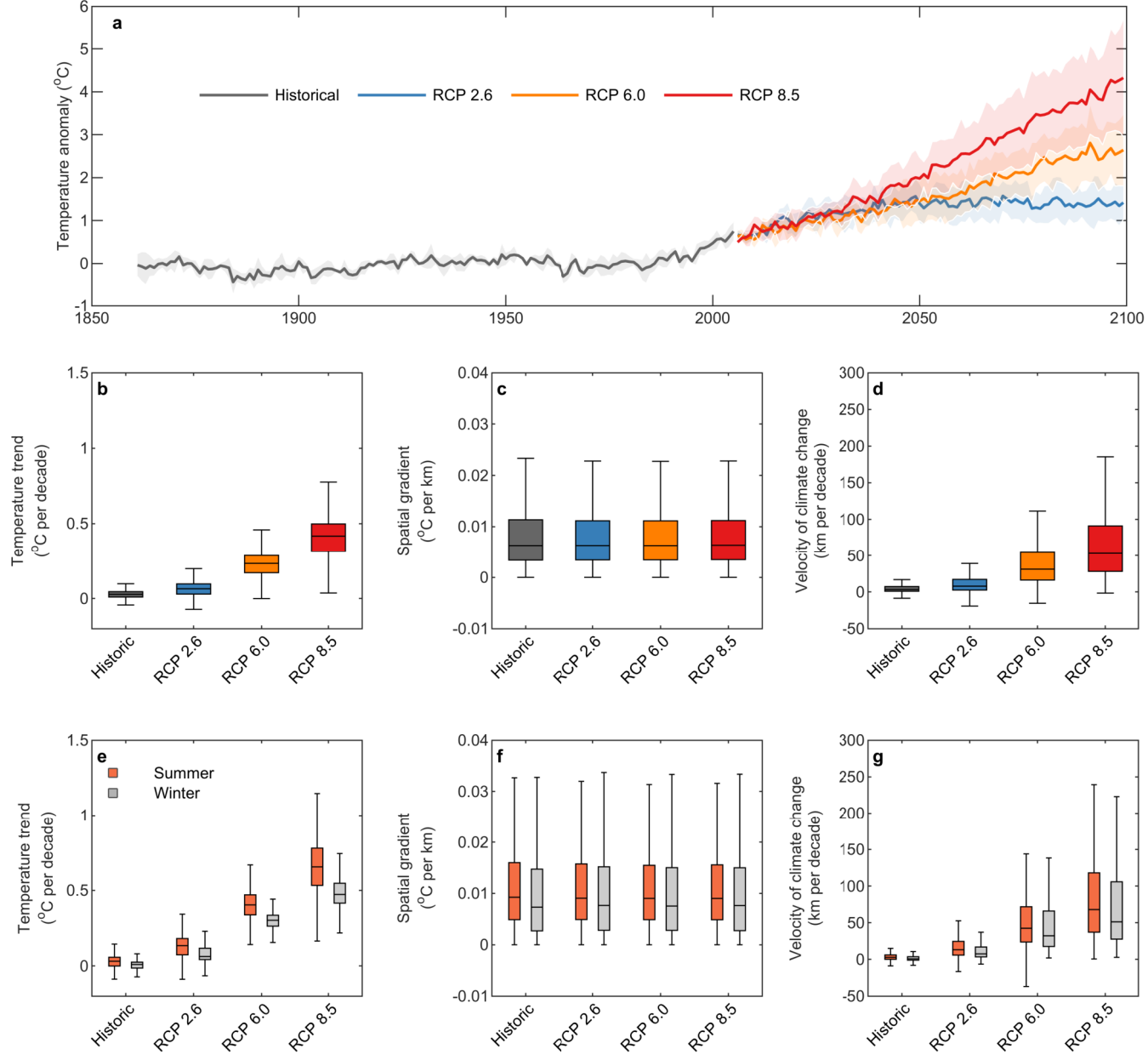
a
Historical
RCP 2.6
RCP 6.0
RCP 8.5
Temperature anomaly (°C)
b
Temperature trend (°C per decade)
c
Spatial gradient (°C per km)
d
Velocity of climate change (km per decade)
e
Summer
Winter
f
g
Historic
RCP 2.6
RCP 6.0
RCP 8.5

References

1. Costanza, R. et al., The value of the world's ecosystem services and natural capital. *Nature* **387**, 253-260 (1997).
2. O'Reilly, C. et al., Rapid and highly variable warming of lake surface waters around the globe. *Geophys. Res. Lett.* **42**, 10773-10781 (2015).
3. Loarie, S. R. et al., The velocity of climate change. *Nature* **462** 1052-1055 (2009).
4. Comte, L. & Grenouillet G., Do stream fish track climate change? Assessing distribution shifts in recent decades. *Ecography* **36**, 1236-1246 (2013).
5. Woolway, R. I. & Merchant, C. J. Worldwide alteration of lake mixing regimes in response to climate change. *Nat. Geosci.* **12**, 271-276 (2019).
6. Till, A. et al., Fish die-offs are concurrent with thermal extremes in north temperate lakes. *Nat. Clim. Change* **9**, 637-641 (2019).
7. Abell, R. et al., Freshwater ecoregions of the world: A new map of biogeographic units for freshwater biodiversity conservation. *BioScience* **58**, 403-414 (2008).
8. Maberly, S.C. et al., Global lake thermal regions shift under climate change. *Nat. Comm*. **11**:1232 (2020).
9. Woolway, R.I. & Merchant, C.J., Intralake heterogeneity of thermal responses to climate change: A study of large northern hemisphere lakes. *J. Geophys. Res. Atmos*. **123**, 3087-3098 (2018).
10. Winslow, L.A. et al., Small lakes show muted climate change signal in deepwater temperatures. *Geophys. Res. Lett*. **42**, 355-361 (2015).
11. Winslow, L.A. et al., Seasonality of change: Summer warming rates do not fully represent effects of climate change on lake temperatures. *Limnol. Oceanogr*. **62**, 2168-2178 (2017).
12. Burrows, M. T. et al., The pace of shifting climate in marine and terrestrial ecosystems. *Science* **334**, 652-655 (2011).
13. Burrows, M. T. et al., Geographical limits to species-range shifts are suggested by climate velocity. *Nature* **507**, 492-495 (2014).
14. Woodward, G. et al., Climate change and freshwater ecosystems: impacts across multiple levels of organization. *Philos. Trans. Royal Soc. B* **365**, 2093-2106 (2010).
15. Woolway, R.I. et al., Warming of Central European lakes and their response to the 1980s climate regime shift, *Clim Change.* **142**, 505-520 (2017).
16. Realis-Doyelle, E. et al., Strong Effects of Temperature on the Early Life Stages of a Cold Stenothermal Fish Species, Brown Trout (Salmo trutta L.). *Plos ONE* **11**(5): e0155487 (2016).
17. Dahlke, F.T., Wohlrab, S., Butzin, M. & Pörtner, H. Thermal bottlenecks in the life cycle define climate vulnerability of fish. *Science* **369**(6499), 65-70 (2020).

277 18. Comte, L. & Olden, J.D. Climatic vulnerability of the world's freshwater and marine fishes.
278 *Nat. Clim. Change* **7**, 718-722 (2017).

279 19. Jones, I. D. et al., Assessment of long-term changes in habitat availability for Arctic charr
280 (*Salvelinus alpinus*) in a temperate lake using oxygen profiles and hydroacoustic surveys.
281 *Freshwater Biol*. **53**, 393-402 (2008).

282 20. Brito-Morales, I. et al. Climate velocity reveals increasing exposure of deep-ocean
283 biodiversity to future warming. *Nat. Clim. Change* **10**, 576-581 (2020).

284 21. Thackeray, S. J. et al., Food web de-synchronization in England's largest lake: an
285 assessment based on multiple phenological metrics. *Glob. Change Biol*. **19**, 3568-3580
286 (2013).

287 22. Walters, A. W. et al., The interaction of exposure and warming tolerance determines fish
288 species vulnerability to warming stream temperatures. *Biol. Lett.* **14**, 2018342 (2018).

289 23. Duarte, H., et al. Can amphibians take the heat? Vulnerability to climate warming in
290 subtropical and temperate larval amphibian communities. *Glob. Change Biol*. **18**, 412-421
291 (2012).

292 24. Rader, R.B., Unmack, P.J., Christensen, W.F., Jiang, X. Connectivity of two species with
293 contrasting dispersal abilities: a test of the isolated tributary hypothesis. *Freshwater Science*
294 **38**, 142-155 (2019).

295 25. Kappes, H. & Haase, P., Slow, but steady: dispersal of freshwater molluscs. *Aquat. Sci.* **74**,
296 1-14 (2012).

297 26. Smith, M.A. & Green, D.M. Dispersal and the metapopulation paradigm in amphibian
298 ecology and conservation: are all amphibian populations metapopulations? *Ecography* **28**,
299 110-128 (2005).

300 27. Comte, L. & Olden, J.D., Fish dispersal in flowing waters: A synthesis of movement- and
301 genetic-based studies. *Fish and Fisheries* **19**, 1063-1077 (2018).

302 28. Zarfl, C. et al., A global boom in hydropower dam construction. *Aquat. Sci.* **7**, 1279-1299
303 (2015).

304 29. Carvajal-Quintero, J. et al., Drainage network position and historical connectivity explain
305 global patterns in freshwater fishes' range size. *Proc. Natl. Acad. Sci* **116**, 13434-13439
306 (2019).

307 30. Strayer, D. L. & Dudgeon, D., Freshwater biodiversity conservation: recent progress and
308 future challenges. *J. N. Amer. Benthol. Soc.* **29**, 344-358 (2010).

309 31. Hughes, J. M. et al., Genes in streams: using DNA to understand the movement of
310 freshwater fauna and their riverine habitat. *Bioscience* **59**, 573-583 (2009).

311 32. Incagnone, G. et al., How do freshwater organisms cross the 'dry ocean'? A review on
312 passive dispersal and colonization process with a special focus on temporary ponds.
313 *Hydrobiologia* **750**, 103-123 (2015).

33. Lenoir, J. et al., Species better track climate warming in the oceans than on land. *Nat. Ecol. Evo*. doi: 10.1038/s41559-020-1198-2 (2020).

Correspondence and requests for materials should be addressed to R. Iestyn Woolway

Acknowledgments: Funding: RIW received funding from the European Union's Horizon 2020 research and innovation programme under the Marie Skłodowska-Curie grant agreement No. 791812. SCM was funded by the NERC Hydroscape Project (NE/N00597X/1). **Author contributions:** Both authors developed the concept of the study. R.I.W performed the modelling. S.C.M and R.I.W led the drafting of the manuscript and both approve the final version of the manuscript; **Competing interests:** The authors do not have any competing financial or non-financial interests to declare.

Data Availability Statement: ERA5 data used in this study are available from https://cds.climate.copernicus.eu/cdsapp#!/dataset/reanalysis-era5-single-levels?tab=overview. The lake model source code is available to download from http://www.flake.igb-berlin.de/. Climate model projections are available at https://www.isimip.org/protocol/#isimip2b.

Methods

Temperature data

Water temperatures from 1979 to 2018 were downloaded from the ECMWF ERA5 reanalysis product at a grid resolution of 0.25° by 0.25°. Surface water temperature of global standing waters were simulated within ERA5 (ref. 34) via the Freshwater Lake model, FLake[35, 36], which is implemented within the Hydrology Tiled ECMWF Scheme for Surface Exchanges over Land (HTESSEL)[37, 38] of the ECMWF Integrated Forecasting System (IFS). The water temperature model is one of the most widely used lake models and has been tested extensively in past studies[5,39]. The lake surface temperatures from ERA5 were also validated in this study with satellite derived lake surface temperatures from the European Space Agency (ESA) Climate Change Initiative (CCI) Lakes project (CCI Lakes; http://cci.esa.int/lakes) which provides, among other things, daily observations of lake surface temperature at a grid resolution of 1/120° for 250 lakes worldwide. From version 1.0 of the CCI Lakes dataset[40], we selected only lakes based on the existence of a 10 × 10 pixel array of pure water surrounding the lake-centre, following the recommendations of ref. 41. For each of these lakes, a 3 × 3 pixel array was then extracted for each day, and the average of these pixels was then calculated prior to comparison with the ERA5 data, which were also extracted for the lake-centre location. The satellite-derived lakes temperatures used in the study were acquired between 2007 and 2018, the period in which most satellite retrievals were available in ESA CCI Lakes. Good agreement was obtained between simulations and satellite-derived observations of lake surface temperature (Extended Data Fig. 1). A detailed description of the surface temperature model and the implementation of surface water temperature in the IFS is provided in ref. 42. The surface water temperature model in the IFS is supported by two climatological fields: (i) an inland water mask, provided by the US Department of Agriculture – Global Land Cover Characteristics (GLCC) data[43], at a nominal resolution of 1 km, which provides the fractions of each surface grid occupied by surface water; (ii) depth, which is specified according to ref. 44 and combined with a global bathymetry dataset, ETOPO1, which is a 1 arc-minute global relief model of Earth's surface that integrates land topography and ocean bathymetry. Surface air temperature over land and sea surface temperatures were also downloaded by ERA5 from 1979 to 2018 at a grid resolution of 0.25° by 0.25°. Thus, the temperature of standing waters, surface air temperature, and sea surface temperature all follow a consistent modelling framework. All data from January 1979 to December 2018, inclusive, were accessed and analysed at an hourly resolution. Annual and seasonal averages, which were used in all velocity calculations, were then calculated from the hourly data. Summer and winter temperatures were calculated for standing waters. Following ref. 2, summer was defined as 1 July - 30 September for lakes situated in the Northern Hemisphere and 1 January - 31 March in the Southern Hemisphere.

Climate model projections

To calculate the velocity of climate change during the 21st century, we used the same water temperature model as in ERA5 but driven by bias-corrected climate projections from four climate models GFDL-ESM2M, HadGEM2-ES, IPSL-CM5A-LR, and MIROC5 for historic (1901-2005) and contemporary to future periods (2006-2099) under three scenarios: RCP 2.6,

6.0, and 8.5. Similar to ref. 5, we downloaded atmospheric forcing data (air temperature at 2 m, wind speed at 10 m, surface solar and thermal radiation, and specific humidity) needed to drive FLake from ISIMIP2b (https://www.isimip.org/protocol/#isimip2b). All climate projection data were available at daily intervals and at a grid resolution of 0.5º. These data were used as inputs to the model after bias-adjustment to the EWEMBI reference dataset[45,46]. To drive the surface water temperature model, lake depths were determined from the Global Lakes and Wetlands Database[47], aggregated from the original 30 arc sec Global Lake Data Base[44,48,49] to a 0.5°-by-0.5° grid lake depth field. The depth dataset used by the lake model (i.e., the average depth of all lakes within a grid), could influence the future projections, given that depth is an important lake attribute influence the thermal response of lakes to climate change[5, 50]. Notably, lakes of different depths within a grid could behave differently than those included here, and is a limitation which should be considered when interpreting these results.

Velocity of Climate Change

Climate velocities (km year^{-1}) were calculated by dividing long-term temperature trends (°C decade^{-1}) by the spatial temperature gradient (°C km^{-1}). Long-term trends of each grid-cell were calculated as the slope of a linear trend model, and the spatial gradients were calculated using a 3x3 grid cell neighborhood. Ultimately, the spatial temperature gradient was calculated as the vector sum of the north-south and east-west temperature gradients. Specifically, the spatial temperature gradient for a focal cell was calculated as the difference in temperature for each northern and southern pair divided by the distance between them[12]. For these calculations we used the *R* package 'Vocc' (ref. 51, 52).

References

34. Hersbach, H. et al., The ERA5 Global Reanalysis. *Quat. J. Roy. Met. Soc.* doi:10.1002/qj.3803 (2020).

35. Mironov, D. Parameterization of lakes in numerical weather prediction: Part 1. Description of a lake mode. COSMO Technical Report, No. 11, Deutscher Wetterdienst, Offenbach am Main, Germany (2008).

36. Mironov, D. et al., Implementation of the lake parameterisation scheme FLake into the numerical weather prediction model COSMO. *Boreal Environ. Res*. **15**, 218–230 (2010).

37. Dutra, E. et al., An offline study of the impact of lakes on the performance of the ECMWF surface scheme. *Boreal Environ. Res.* **15**, 100-112 (2010).

38. Balsamo, G. et al., On the contribution of lakes in predicting near-surface temperature in a global weather forecasting model. *Tellus A* **64**, 15829 (2012).

39. Le Moigne, P., Colin, J. & Decharme, B. Impact of lake surface temperatures simulated by the FLake scheme in the CNRM-CM5 climate model. *Tellus A* **68**, 31274 (2016).

40. Crétaux, J.-F., Merchant, C.J., Duguay, C. et al. ESA Lakes Climate Change Initiative (Lakes_cci): Lake products, Version 1.0. Centre for Environmental Data Analysis, 08 June 2020, doi: 10.5285/3c324bb4ee394d0d876fe2e1db217378 (2020).

41. Schneider, P. & Hook, S.J. Space observations of inland water bodies show rapid surface warming since 1985. *Geophys. Res. Lett*. **37**(22) (2010).

42. ECMWF, IFS Documentation CY45R1, Part IV: Physical processes. Available at https://www.ecmwf.int/node/18714 (2018).

43. Loveland, T. R. et al., Development of a global land cover characteristics database and IGBP DISCover from 1km AVHRR data. *Int. J. Remote Sens.* **21**, 1303-1330 (2000).

44. Kourzeneva, E. External data for lake parameterization in Numerical Weather Prediction and climate modelling. *Boreal Env. Res.* **15**, 165-177 (2010).

45. Frieler, K. et al. Assessing the impacts of 1.5°C global warming - Simulation protocol of the Inter-Sectoral Impact Model Intercomparison Project (ISIMIP2b). Geoscientific Model Development 10, 4321–4345 (2017).

46. Lange, S. EartH2Observe, WFDEI and ERA-Interim data Merged and Bias-corrected for ISIMIP (EWEMBI). V.1.1. GFZ Data Services. http://doi.org/10.5880/pik.2019.004. Accessed 18-04-2019. (2019).

47. Lehner, B. & Döll, P., Development and validation of a global database of lakes, reservoirs and wetlands. *J. Hydrol*. **296**, 1–22 (2004).

48. Subin, Z. M., Riley, W. J. & Mironov, D., An improved lake model for climate simulations: Model structure, evaluation, and sensitivity analyses in CESM1. *Journal of Advances in Modeling Earth Systems* **4**, 1–27 (2012).

49. Choulga, M., Kourzeneva, E., Zakharova, E. & Doganovsky, A., Estimation of the mean depth of boreal lakes for use in numerical weather prediction and climate modelling. *Tellus, Series A: Dynamic Meteorology and Oceanography* **66** (2014).

50. Woolway, R.I., Merchant, C.J., Amplified surface temperature response of cold, deep lakes to inter-annual air temperature variability, *Sci. Rep* **7**: 4130 (2017).

51. R Development Core Team, R: A language and environment for statistical computing, R Foundation for Statistical Computing, Vienna, Austria. [Available at http://www.R-project.org/.] (2018).

52. Molinos, J.G. et al., VoCC: An R package for calculating the velocity of climate change and related climatic metrics. *Methods in Ecology and Evolution* **10**, 2195-2202 (2019).

Extended Data

Extended Data Fig. 1 | Validation of simulated lake surface temperatures. Comparison of simulated and satellite-derived surface water temperatures for 196 lakes (2007-2018) from the ESA CCI Lakes dataset. Shown are comparisons of the average open-water temperatures for the lake-centre pixels.

Extended Data Fig. 2 | The velocity of climate change in European standing waters. Shown for standing waters in Europe are **(a)** the surface water temperature trend, **(b)** the two-dimensional spatial gradient of surface water temperature change, and **(c)** the velocity of climate change during the 1979 to 2018 period. White regions represent those where standing waters are absent within the global database.

Extended Data Fig. 3 | Global relationship between the spatial temperature gradient and elevation. Shown is a comparison of **(a)** the two-dimensional spatial gradient of surface water temperature change, and **(b)** elevation. White regions represent those where standing waters are absent within the global database.

Extended Data Fig. 4 | Comparison of the velocity of climate change and the spatial elevation gradient. Shown is the relationship between the velocity of climate change in the surface of inland surface waters and the two-dimensional spatial gradient of elevation change. Specifically, we show that climate change velocities are greater at sites with low elevation gradients. Thus, steep sites which show rapid change in elevation, experience lower climate velocities. Each box represents the interquartile range, the horizontal line is the median, and the whiskers are 1.5 times the interquartile range.

Extended Data Fig. 5 | Historic and future projections of global surface air temperature. Temporal change in annual surface air temperature anomalies (relative to 1951-1980) from 1861-2099 showing the historic period (1861-2005), with contemporary to future climate projections (2006-2099) under three representative greenhouse gas concentration scenarios (RCPs 2.6, 6.0, 8.5). The thick lines show the average of four global climate models (MIROC5, IPSL-CM5A-LR, GFDL-ESM2M, HadGEM2-ES), and the shaded regions represent the standard deviation.

Extended Data Fig. 6 | Global variations in the velocity of climate change from 2006-2099 relative to 1861-2005. Shown are the differences in the simulated velocity of climate change between the historic (1861-2005) and the contemporary to future (2006-2099) period (i.e., future minus historic) under RCP 8.5. Results are shown for the lake model forced by four global climate models (MIROC5, IPSL-CM5A-LR, GFDL-ESM2M, HadGEM2-ES). White regions represent those where the difference in climate velocities are negligible.

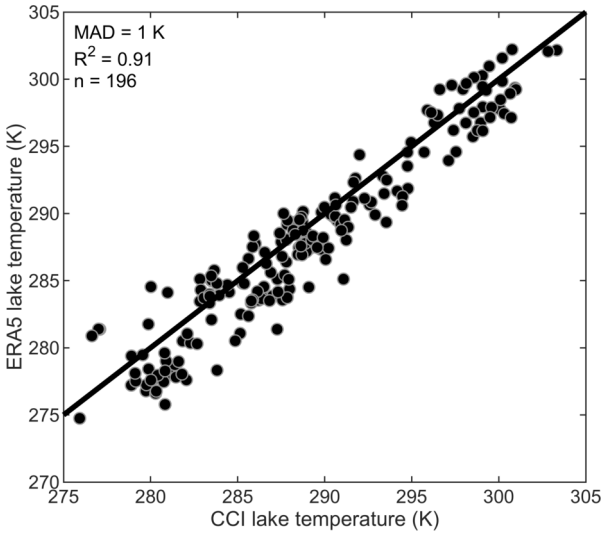
MAD = 1 K
R2 = 0.91
n = 196
ERA5 lake temperature (K)
CCI lake temperature (K)
305
300
295
290
285
280
275
270
275
280
285
290
295
300
305

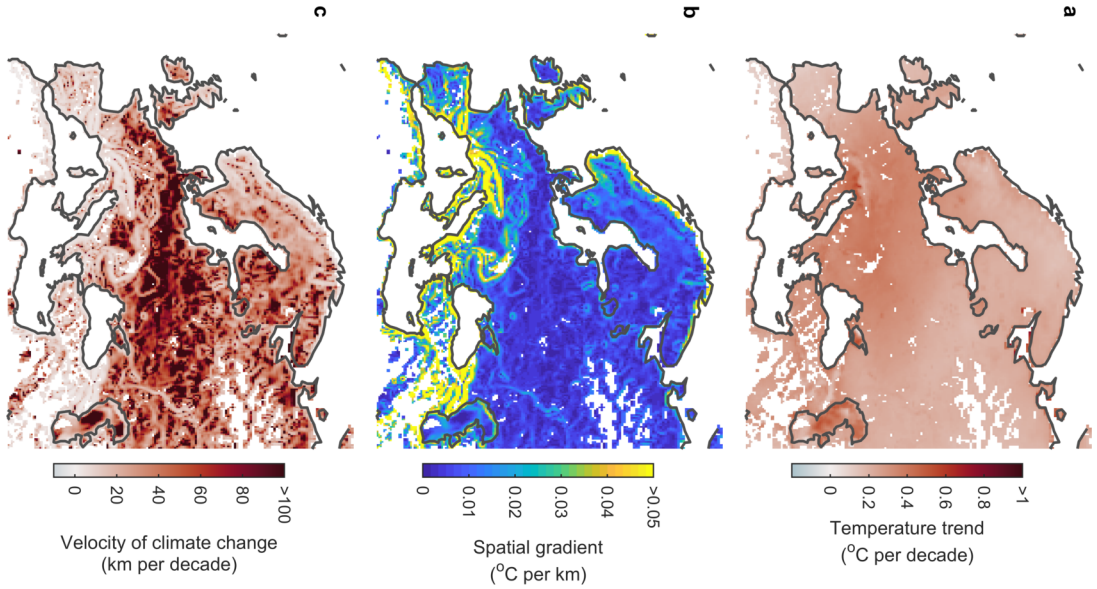
c
b
a
0
20
40
60
80
>100
Velocity of climate change
(km per decade)
0
0.01
0.02
0.03
0.04
>0.05
Spatial gradient
(°C per km)
0
0.2
0.4
0.6
0.8
>1
Temperature trend
(°C per decade)

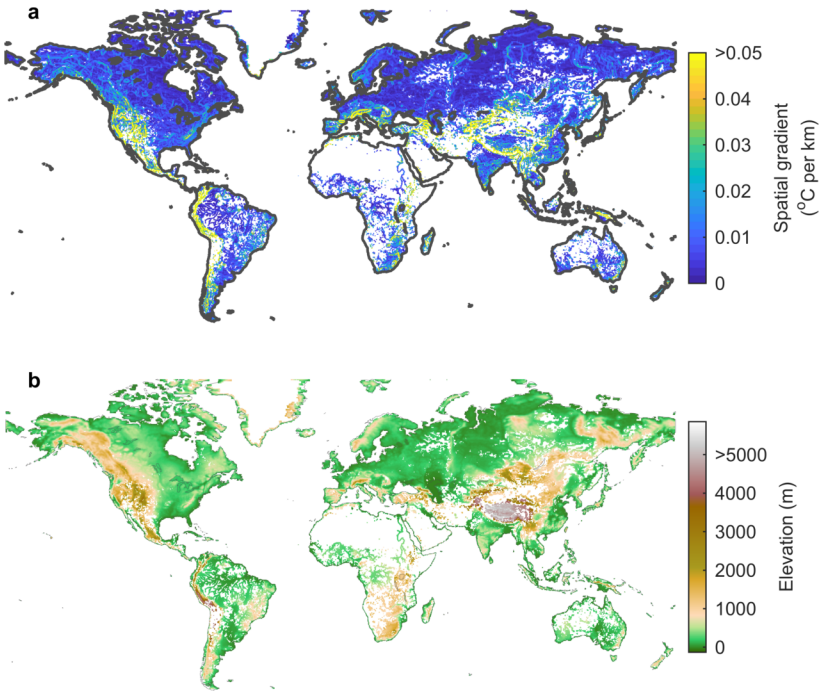
a
>0.05
0.04
0.03
0.02
0.01
0
Spatial gradient
(°C per km)
b
>5000
4000
3000
2000
1000
0
Elevation (m)

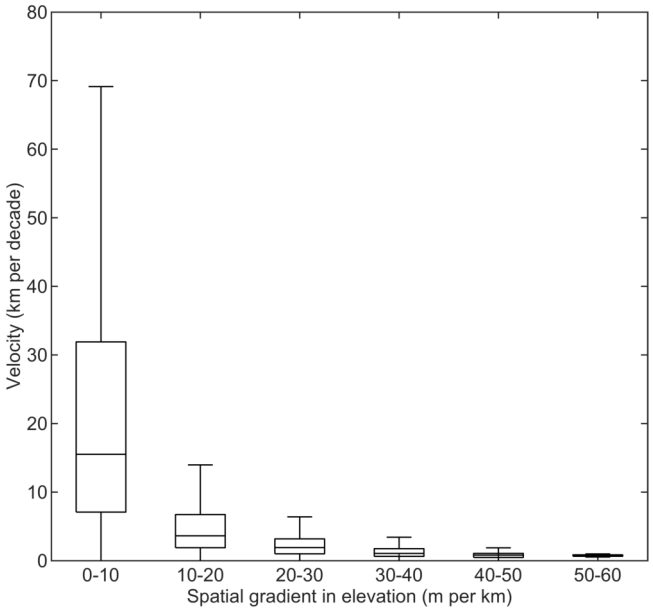
80
70
60
50
40
30
20
10
0
Velocity (km per decade)
0-10
10-20
20-30
30-40
40-50
50-60
Spatial gradient in elevation (m per km)

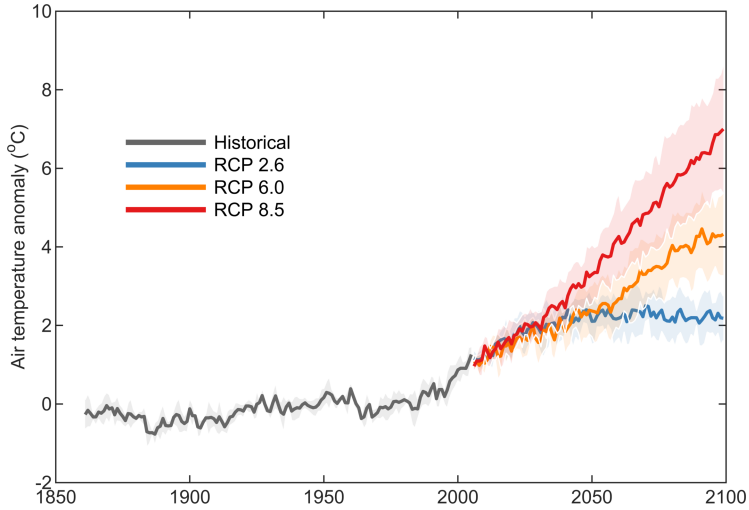
Historical
RCP 2.6
RCP 6.0
RCP 8.5
Air temperature anomaly (°C)
10
8
6
4
2
0
-2
1850
1900
1950
2000
2050
2100

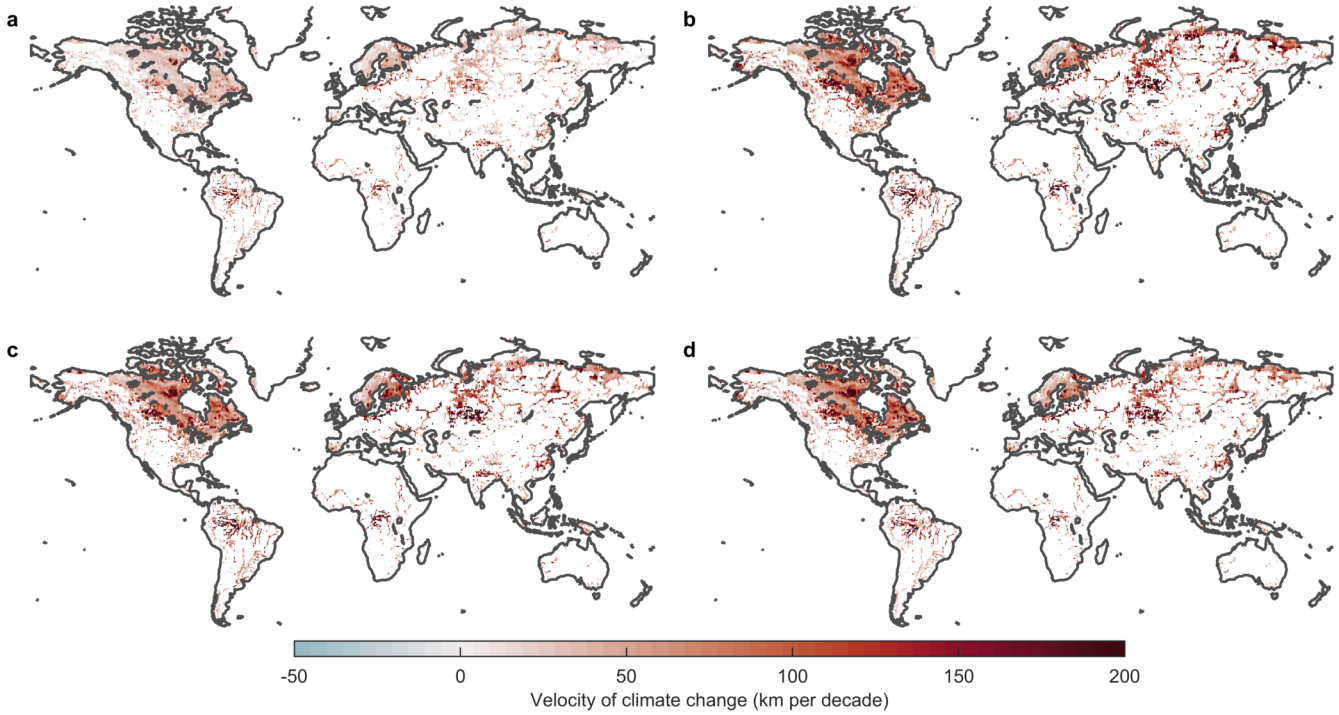
a
b
c
d
-50
0
50
100
150
200
Velocity of climate change (km per decade)